Proofs to: Dr G. A. Solan

Department of Chemistry

University of Leicester

University Road

Leicester LE1 7RH

REVISED MANUSCRIPT

Bis(iminopyridyl)phthalazine as a Sterically Hindered Compartmental Ligand for an M_2 (M = Co, Ni, Fe, Zn) Centre; Applications in Ethylene Oligomerisation

Nicky Savjani, Kuldip Singh and Gregory A. Solan*

Department of Chemistry, University of Leicester, University Road, Leicester LE1 7RH, UK

* Corresponding author. E-mail: gas8@leicester.ac.uk (G.A. Solan). Fax: +44 (0)116 252 3789

† Electronic supplementary information (ESI) available: CCDC 1401482-1401487. For ESI and crystallographic data in CIF or other electronic format see DOI: ……..

ABSTRACT

The new bis(iminopyridyl)phthalazine ligand, 1,4-{(2,6-*i*-$Pr_2C_6H_3$)N=CMe)C_5H_3N}$_2C_8H_4N_2$ (**L**), has been prepared in good yield using a combination of palladium-mediated cross coupling and condensation strategies. Reaction of **L** with three equivalents of CoX_2 (X = Cl, Br) in *n*-BuOH at elevated temperature generates, on crystallisation from bench acetonitrile, the paramagnetic tetrahalocobaltate salts [(**L**)$Co_2X(\mu\text{-}X)(NCMe)_m(OH_2)_n$]($CoX_4$) (X = Cl, *m* = 2, *n* = 1 **1a**; X = Br, *m* = 2, *n* = 0 **1b**) as acetonitrile or mixed acetonitrile/aqua adducts; a similar product is obtained from the reaction of $FeCl_2$ with **L** and has been tentatively assigned as [(**L**)$Fe_2Cl(\mu\text{-}Cl)(OH_2)_3$]($FeCl_4$) (**2**). By contrast, reaction of **L** with NiX_2(DME) (X = Cl, Br; DME = 1,2-dimethoxyethane), under similar reaction conditions, affords the halide salts [(**L**)$Ni_2X_2(\mu\text{-}X)(OH_2)_2$](X) (X = Cl **3a**, X = Br **3b**) as aqua adducts. Structural determinations on **1** and **3** reveal **L** to adopt a bis(tridentate) bonding mode allowing the halide-bridged metal centres to assemble in close proximity (M···M *range*: 3.437 – 3.596 Å). Unexpectedly, on reaction of **L** with $ZnCl_2$, the neutral bimetallic [(**L**)Zn_2Cl_4] (**4b**) complex is formed in which the $ZnCl_2$ units fill inequivalent binding sites within **L** (*viz*. the N_{phth},N_{py},N_{im} and N_{py},N_{im} pockets). Complex **4b** could also be obtained by the sequential addition of $ZnCl_2$ to **L** to form firstly monometallic complex [(**L**)$ZnCl_2$] (**4a**) and then on further $ZnCl_2$ addition **4b**; the fluxional behaviour of diamagnetic **4a** and **4b** is also reported. On activation with excess methylaluminoxane (MAO), **1** – **3** display modest activities for alkene oligomerisation forming low molecular weight waxes with methyl-branched products predominating for the nickel systems (**3**). On the other hand, the iron catalyst (**2**) gives exclusively α-olefins while the cobalt systems (**1**) are much less selective affording equal mixtures of α-olefins and internal olefins along with lower levels of vinylidenes and tri-substituted alkenes. Single crystal X-ray structures are reported for **L**, **1a**, **1b**, **3a**, **3b** and **4**.

Keywords:
Cobalt,
Iron,
Nickel,
Zinc,
Ethene oligomerisation,
Coordination chemistry.

1. Introduction

Recent years have seen an upsurge in interest in the development of suitably tailored ligand frameworks capable of housing more than one olefin oligomerisation- or polymerisation-active metal centre in close proximity [1]. This bioinspired strategy [2] has led to a raft of bimetallic (both early [1,3] and late [1,4-7] transition metals) catalysts being reported bearing a range of binucleating ligands that can display different degrees of flexibility and enforce a broad range of metal-metal separations. With regard to late transition metal catalysts (*e.g.*, Fe, Co, Ni), beneficial effects reported so far include increased stability and activity [8], inhibition of Lewis base deactivation [9] and increased polar comonomer incorporation [10]. Notably, however, reports of rigid architectures that can enforce the late metal ions into separations of less than 4 Å are more limited due, in part, to the scarcity of ligand manifolds that can impart the necessary steric and electronic properties [11].

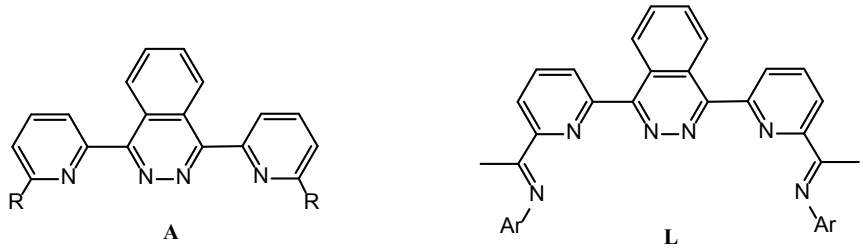

A (R = H, COO^-, 2-[1,8]-naphthyridine) **L** (this work, Ar = 2,6-diisopropylphenyl)

Fig. 1. Compartmental ligands based on 1,4-dipyridinyl-substituted phthalazines (**A**) and **L**

Compartmental ligands based on a central phthalazine moiety functionalised at its 1,4-positions have been widely employed in coordination chemistry and examples of donor arms that have been tethered to this core include triazoles [12], alkylphosphines [13], alkylimines [14], alkylpyridines [15] and alkylimadazoles [16]. By contrast, reports of 1,4-dipyridyl-phthalazines and its substituted pyridyl derivatives are less common [17]. For example, 1,4-dipyridyl-phthalazines appended with carboxylates and napthyridine donors (**A** in Fig. 1) have been reported for ruthenium and highlight the capacity of these ligand sets to act as bis(tridentate) ligands allowing metal-metal separations of between 3.576 and 3.671 Å.

Herein, we are concerned with developing a 1,4-dipyridyl-phthalazine that contains two bulky *N*-arylimine end groups with a view to exploring its ability to act as rigid binucleating ligand for two closely located 3d metal centres. In particular, we report the synthesis and characterisation

of cobalt(II), iron(II) and nickel(II) halide complexes of 1,4-{(2,6-*i*-$Pr_2C_6H_3$)N=CMe)C_5H_3N}$_2C_8H_4N_2$ (**L**) (Fig. 1) and their performance in ethylene oligomerisation. To complement the coordination chemistry study, we also report the corresponding zinc(II) halide chemistry with view to exploring the solution state properties of these diamagnetic species.

2. Results and discussion

2.1. Ligand synthesis

The bis(iminopyridine)phthalazine, 1,4-{(2,6-*i*-$Pr_2C_6H_3$)N=CMe)C_5H_3N}$_2C_8H_4N_2$ (**L**), can be prepared by reacting 1,4-{(O=CMe)C_5H_3N}$_2C_8H_4N_2$ with 2,6-diisopropylaniline (as reagent and solvent) at elevated temperature (*ca.* 230 °C) over a 35 minute reaction time. The precursor carbonyl compound, 1,4-{(O=CMe)C_5H_3N}$_2C_8H_4N_2$ [17b] is not commercially available and is synthesised by a palladium-mediated cross-coupling of 2-(Bu_3Sn)-6-{C(Me)OCH_2CH_2O}C_5H_3N with 1,4-dibromophthalazine (Scheme 1); the overall synthetic approach being based on a general method for preparing 2,6-oligopyridylimines [18].

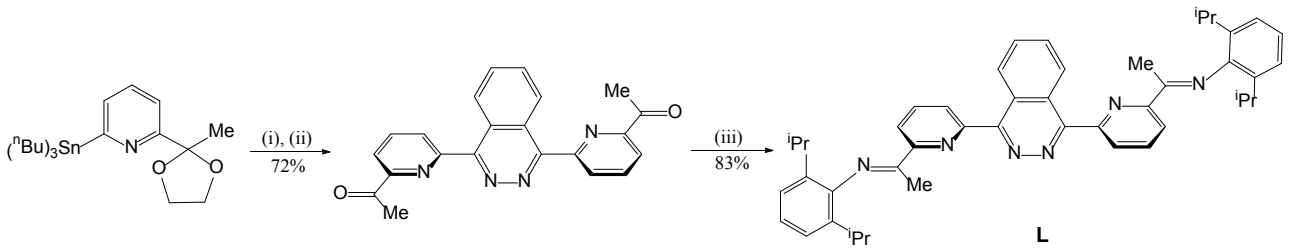

Scheme 1. *Reagents and conditions*: (i) $C_8H_4N_2Br_2$, $Pd(PPh_3)_4$ (8 mol%), CuBr (16 mol%), toluene, 100 °C, 72 h; (ii) HCl (4M), 60 °C, 12 h; (iii) 2,6-*i*-$Pr_2C_6H_3NH_2$, 230 °C, cat. H^+.

Compound **L** displays a protonated molecular ion peak in its ESI mass spectrum and exhibits a $\upsilon(C{=}N)_{imine}$ absorption band at 1645 cm^{-1} in its IR spectrum. In the ^1H NMR spectrum the equivalent C*Me*=N protons are seen as a singlet at δ 2.27 while the *C*Me=N carbon is found at δ 165.9 in the $^{13}C\{^1H\}$ NMR spectrum. Further confirmation of the composition of **L** was achieved in the form of a single crystal X-ray determination.

L crystallises as three independent molecules (*A*, *B* and *C*) which differ most notably in the relative inclination of the central phthalazine group to the adjacent pyridine units. A view of molecule *A* is depicted in Figure 2; selected bond lengths and angles are collected for all three in

Table 1. Crystals suitable for the X-ray determination were grown by slow evaporation of a saturated acetonitrile solution. The molecular structure of **L** consists of a central phthlazinyl group linked at its 1- and 4-positions by two pyridylimine units. Within each unit, the pyridyl and imine moieties are essentially coplanar [*tors.* N(1)-C(13)-C(15)-N(2) 9.6°$_A$, *B* 5.8°$_B$, 4.8°$_C$; N(5)-C(32)-C(33)-N(6) 13.9°$_A$, 6.2°$_B$, 3.2°$_C$] with the respective nitrogen atoms disposed mutually *trans*. In contrast, the phthlazinyl and neighbouring pyridine groups are inclined towards orthoganality in molecule *A* [*tors.* N(2)-C(19)-C(20)-N(3) 79.8°; N(4)-C(27)-C(28)-N(5) 75.7°], whilst in molecules *B* and *C* some significant deviations are apparent [*tors.* N(2)-C(19)-C(20)-N(3) 44.2°$_B$, 79.6°$_C$; N(4)-C(27)-C(28)-N(5) 75.4°$_B$, 53.5°$_C$]. The C-N$_{imine}$ bond lengths within all three independent molecules [*range:* 1.231(11)-1.308(12) Å] are consistent with double bond character with the chain end *N*-aryl rings adopting *pseudo*-perpendicular arrangements with respect to the adjacent imino units [*tors.* C(13)-N(1)-C(1)-C(2) 85.0°$_A$, 83.0°$_B$, 83.5°$_C$, C(33)-N(6)-C(35)-C(36) 78.6°$_A$, 87.2°$_B$, 87.1°$_C$].

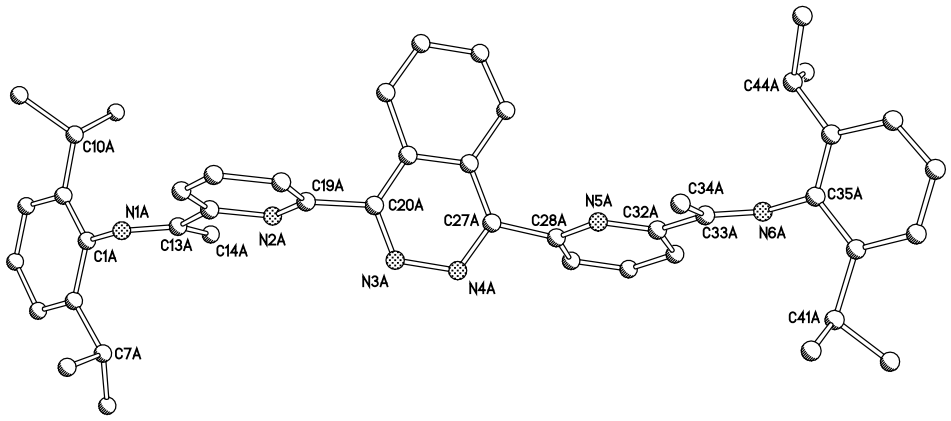

Fig. 2. Molecular structure of **L** (*molecule A*) including a partial atom numbering scheme. All hydrogen atoms been omitted for clarity.

Table 1
Selected bond distances (Å) and angles (°) for **L**

	Molecule A	*Molecule B*	*Molecule C*
Bond lengths			
C(13)-N(1)	1.236(11)	1.231(11)	1.283(11)
C(33)-N(6)	1.308(12)	1.251(11)	1.307(11)
C(19)-C(20)	1.502(13)	1.486(13)	1.488(13)
C(27)-C(28)	1.502(13)	1.513(13)	1.513(13)
N(3)-N(4)	1.419(10)	1.370(10)	1.386(11)
Bond angles			
C(14)-C(13)-N(1)	123.6(9)	127.9(10)	126.2(9)
C(34)-C(33)-N(6)	125.2(10)	125.6(10)	124.4(10)
N(3)-C(20)-C(19)	113.0(10)	114.4(9)	112.5(9)
N(4)-C(27)-C(28)	114.6(10)	117.2(9)	113.9(9)

2.2. Complexation

2.2.1. Cobalt(II) and iron(II) halide complexes

Treatment of **L** with three equivalents of CoX_2 (X = Cl, Br) in *n*-BuOH at elevated temperature gave, on crystallisation from bench acetonitrile, the tetrahalometallate salts, $[(\mathbf{L})Co_2X(\mu\text{-}X)(NCMe)_m(OH_2)_n](CoX_4)$ (X = Cl, *m* = 2, *n* = 1 **1a**; X = Br, *m* = 2, *n* = 0 **1b**), as brown/green plates in good yield (Scheme 2). Both complexes have been characterised by FAB mass spectrometry, IR spectroscopy, elemental analyses, magnetic measurements (see experimental section) and single crystal X-ray determinations.

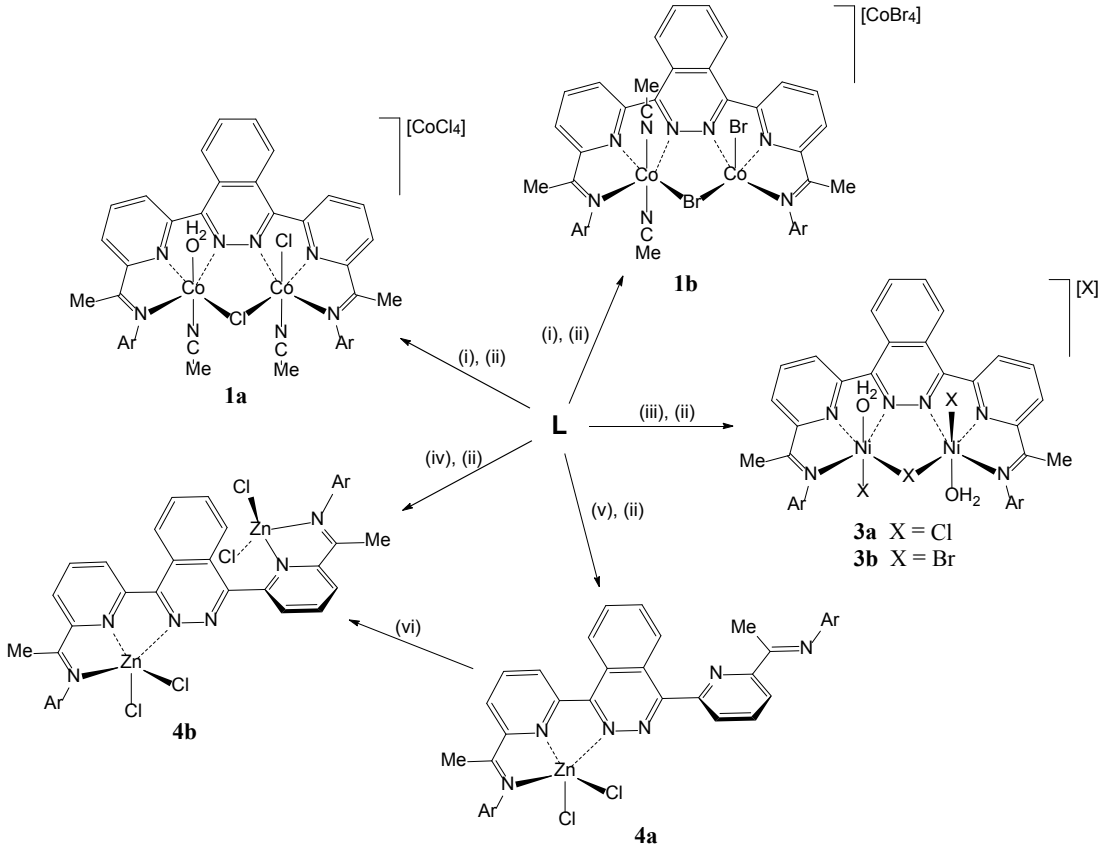

Scheme 2. *Reagents and conditions*: (i) 3 CoX_2 (X = Cl, Br), *n*-BuOH, 95 °C, 12 h; (ii) MeCN-H_2O, heat; (iii) 2 NiX_2(DME) (X = Cl, Br), *n*-BuOH, 95 °C, 12 h; (iv) 2 $ZnCl_2$, *n*-BuOH, 95 °C, 12 h; (v) $ZnCl_2$, *n*-BuOH, 95 °C, 4 h; (vi) $ZnCl_2$, MeCN, RT, 12 h (Ar = 2,6-*i*-$Pr_2C_6H_3$)

The molecular structures of **1a** and **1b** are similar and will be discussed together. Perspective views of **1a** and **1b** are given in Figures 3 and 4; selected bond distances and angles are listed in Tables 2 and 3. Both structures consist of a dicationic unit charge balanced by a discrete tetrahalocobaltate dianion. Within the dicationic unit the Co(μ-X)CoX core is housed within the two neighbouring N_{phth}-N_{py}-N_{im} tridentate binding domains in **L**. At Co(1) in **1a**, a molecule of

acetonitrile and a molecule of water are disposed *trans* to complete a distorted octahedral environment, while in **1b** the water molecule has been replaced by an acetonitrile ligand. At Co(2) a six-coordinate geometry is also observed for **1a**, this time with an acetonitrile molecule *trans* to a terminal chloride ligand. In contrast, the geometry at Co(2) in **1b** can best be described as distorted square pyramidal [$\tau = 0.23$ (where $\tau = 0$ represents ideal square-based pyramidal and $\tau = 1$ trigonal bipyramidal)] [19], with Br(2) occupying the apical site. The nitrogen-metal distances within each *N,N,N*-chelate are uneven with the central N_{py}-Co distance being the shortest [2.067(7), 2.050(6) (**1a**) Å; 2.060(5), 2.051(6) (**1b**) Å] and the interior N_{phth}-Co group the longest [2.154(6), 2.151(7) (**1a**) Å; 2.156(5), 2.145(6) (**1b**) Å]. In **1a** an intramolecular hydrogen bonding interaction between the aqua ligand and Cl(2) [H(1)···Cl(2) 2.238 Å] is also noticeable. Between structures the exchange of a bridging chloride for a bridging bromide has the effect of elongating the metal-metal separation [3.483 (**1a**) *vs.* 3.596 (**1b**) Å]. Some distortion within the pyradazine ring is evident in **1b** [*tors*: C(20)-C(21)-C(26)-C(27) 11.3°] which is less pronounced in **1a** [4.2°]; this is likely due to a combination of the mixed coordination geometries in **1b** and the increased transannular metal separation. The coordinated imine groups [1.276(9), 1.288(10) (**1a**); 1.280(8), 1.286(8) (**1b**) Å] are virtually co-planar with their neighbouring pyridine units with the *N*-aryl units tilted towards orthogonality [*tors.* C(2)-C(1)-N(1)-C(13) 76.18° (**1**), 71.77° (**2**)]. There are no intermolecular contacts of note.

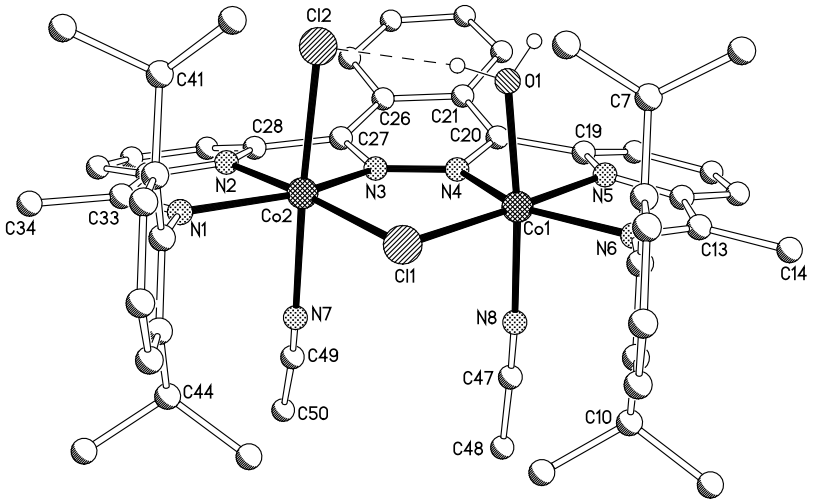

Fig. 3. Molecular structure of the dicationic unit in **1a** including a partial atom numbering scheme. All hydrogen atoms, except for H(1) and H(1a), have been omitted for clarity.

Table 2
Selected bond distances (Å) and angles (°) for **1a**

Bond lengths			
Co(1)-N(4)	2.154(6)	Co(2)-N(1)	2.136(7)
Co(1)-N(5)	2.067(7)	Co(2)-N(2)	2.050(6)
Co(1)-N(6)	2.130(6)	Co(2)-N(3)	2.151(7)
Co(1)-N(8)	2.096(7)	Co(2)-N(7)	2.325(8)
Co(1)-O(1)	2.101(5)	Co(2)-Cl(1)	2.340(2)
Co(1)-Cl(1)	2.354(3)	Co(2)-Cl(2)	2.418(3)
Co(1)···Co(2)	3.483	C(33)-N(1)	1.276(9)
C(13)-N(6)	1.288(10)		
	range Co(3)-Cl (dianion): 2.270(3)-2.314(3)		
Bond angles			
N(4)-Co(1)-N(6)	150.0(3)	N(3)-Co(2)-N(1)	151.2(2)
N(5)-Co(1)-N(6)	77.0(3)	N(3)-Co(2)-N(2)	74.1(2)
N(4)-Co(1)-N(5)	73.2(3)	N(2)-Co(2)-N(1)	77.4(3)
N(5)-Co(1)-Cl(1)	175.84(2)	N(2)-Co(2)-Cl(1)	173.0(2)
O(1)-Co(1)-N(8)	171.9(2)	N(7)-Co(2)-Cl(2)	166.9(2)
Co(1)-Cl(1)-Co(2)	95.82(10)		

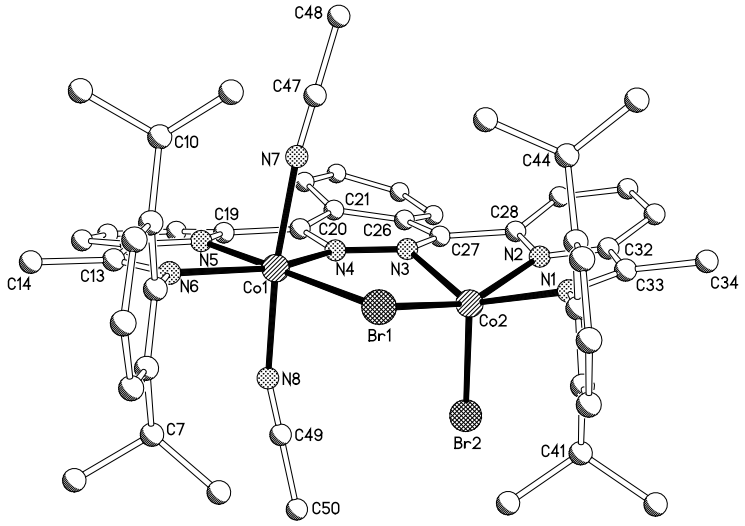

Fig. 4. Molecular structure of the dicationic unit in **1b** including a partial atom numbering scheme. All hydrogen atoms have been omitted for clarity.

Table 3 Selected bond distances (Å) and angles (°) for **1b**

Bond lengths			
Co(1)-N(4)	2.156(5)	Co(2)-N(1)	2.112(6)
Co(1)-N(5)	2.060(5)	Co(2)-N(2)	2.051(6)
Co(1)-N(6)	2.147(6)	Co(2)-N(3)	2.145(6)
Co(1)-N(7)	2.072(7)	Co(2)-Br(1)	2.4728(12)
Co(1)-N(8)	2.130(7)	Co(2)-Br(2)	2.4035(13)
Co(1)-Br(1)	2.4923(12)	C(33)-N(1)	1.286(8)
C(13)-N(6)	1.280(8)	Co(1)···Co(2)	3.596
	range Co(3)-Br (dianion): 2.4120(13)-2.4478(14)		
Bond angles			
N(4)-Co(1)-N(6)	151.8(2)	N(3)-Co(2)-N(1)	141.3(2)
N(5)-Co(1)-N(6)	77.0(2)	N(3)-Co(2)-N(2)	73.5(2)
N(4)-Co(1)-N(5)	74.8(2)	N(2)-Co(2)-N(1)	76.8(2)
N(5)-Co(1)-Br(1)	175.89(17)	N(2)-Co(2)-Br(1)	155.03(17)
N(7)-Co(1)-N(8)	170.3(2)	Br(1)-Co(2)-Br(2)	109.28(5)
Co(1)-Br(1)-Co(2)	92.80(4)		

Both **1a** and **1b** exhibit, in their positive FAB mass spectra, fragmentation peaks corresponding to [(**L**)Co_2X_2], [(**L**)Co_2X] and [(**L**)CoX] (X = Cl, Br). Unexpectedly, a peak attributable to [(**L**)Co_2X_3] is also visible (the apparent result of halide addition to the **L**Co_2X_2 core in **1**) in both spectra. The origin of this additional halide is unclear as the formulation for **1a** and **1b** as a dication-$[CoX_4]^{2-}$ pair is supported by the microanalytical data. Furthermore, their negative FAB mass spectra confirm the presence of a tetrahalocobaltate dianion with a [CoX_3] peak clearly visible for both complexes. In their IR spectra the $\upsilon(C{=}N)_{imine}$ band is shifted *ca.* 45 cm^{-1} to lower in wavenumber in comparison with **L** consistent with metal coordination; weak absorption bands attributable to coordinated acetonitrile ligands can be seen in both complexes at *ca*. 2283 cm^{-1}.

The related reaction of **L** with $FeCl_2$ was also explored and gave on recrystallisation from a mixture of dichloromethane and hexane a navy blue microcrystalline material that has tentatively been assigned [(**L**)$Fe_2Cl(\mu\text{-}Cl)(OH_2)_3$]($FeCl_4$) (**2**). Unfortunately crystals suitable for a single crystal X-ray diffraction study could not be obtained. Nevertheless the spectroscopic and spectrometric properties of **2** resemble those of **1** with the positive FAB mass spectrum indicating fragmentation peaks corresponding to [(**L**)Fe_2Cl_2] and [(**L**)FeCl], while the negative FAB mass spectrum showed a peak for [$FeCl_3$]. Moreover, the microanalytical data supports the composition proposed for **2**.

*2.2.2 Nickel(II) halide complexes (**3**)*

Similar treatment of **L** with three equivalents of NiX_2(DME) (X = Cl, Br; DME = 1,2-dimethoxyethane) in *n*-BuOH at elevated temperature gave, on prolonged standing in bench acetonitrile, [(**L**)$Ni_2X_2(\mu\text{-}X)(OH_2)_2$](X) (X = Cl **3a**, X = Br **3b**) as red-brown crystals, in moderate yield (Scheme 2). The yield of **3a** and **3b** was subsequently improved by using the corresponding 2:1 stoichiometry for NiX_2(DME) to **L**. Both complexes have been characterised using FAB mass spectrometry, IR spectroscopy, elemental analyses and magnetic measurements

(see experimental section). In addition, **3a** and **3b** have been the subject of single crystal X-ray diffraction studies.

Perspective views of **3a** and **3b** are given in Figure 5; selected bond distances and angles for both species are collected in Table 4. Each structure comprises a bimetallic monocationic unit charge balanced by a halide counter-anion. In the case of **3a** a centrosymmetric dinuclear core is adopted while in **3b** this symmetry is absent, otherwise both structures show similar features. Within the cationic unit the two nickel centres are accommodated in the two tridentate N_{phth}-N_{py}-N_{im} pockets of **L** and bridged by a single halide ligand facilitating metal-metal separations of 3.437 (**3a**) and 3.569 (**3b**) Å. Each metal centre is further coordinated by mutually *trans*-disposed halide and water ligands to give two vertex-sharing octahedral geometries. Both water molecules undergo a hydrogen bonding interaction with a neighbouring halide ligand [H(1)···Cl(2A) 2.298 Å (**3a**); H(2)···Br(1) 2.689 Å, H(1)···Br(2) 2.542 Å (**3b**)] and, in addition, one or both aqua ligands undergo hydrogen bonding interactions with the halide counterion [H(2)···Cl(2A) 2.176 Å (**3a**), H(1A)···Br(4A) 2.457 Å (**3b**)]. As with **1a** and **1b** there is some twisting within the pyradazine ring which is even more significant in **3** [*tors*: C(20)-C(21)-C(21A)-C(20A) 12.9° (**3a**), C(20)-C(21)-C(26)-C(27) 13.4° (**3b**)]; it seems plausible that the steric influence imparted by the addition of an extra halide ligand to the M(μ-X)MX core in **1** is influencing this distortion.

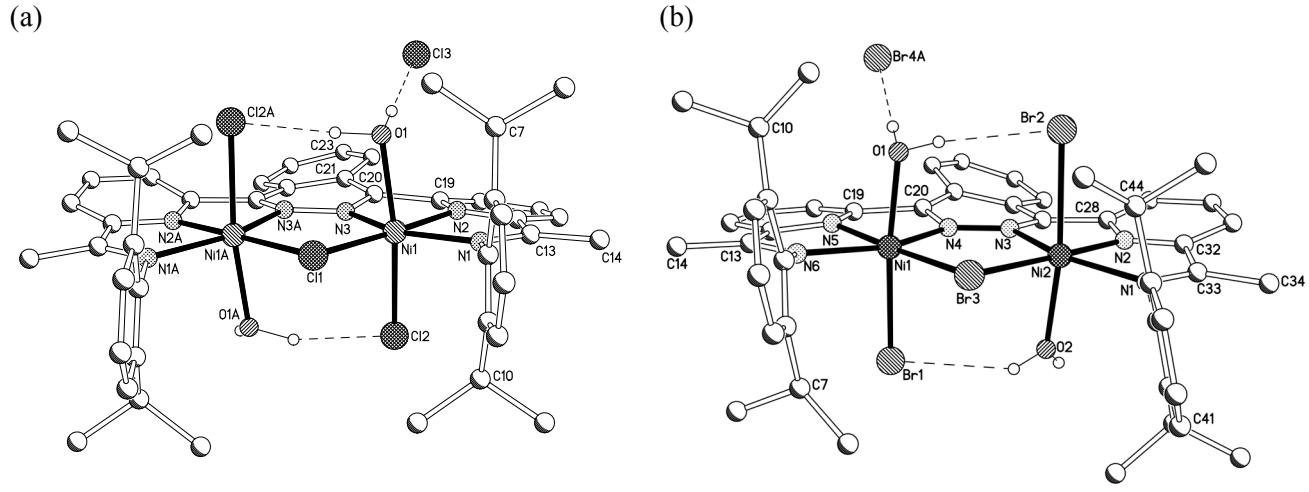

Fig. 5. Molecular structures of (a) **3a** and (b) **3b**, including a partial atom numbering scheme. All hydrogen atoms, apart from those belonging to the waters, have been omitted for clarity.

Table 4
Selected bond distances (Å) and angles (°) for **3a** and **3b**

3a[a]		**3b**			
Bond lengths					
Ni(1)-N(1)	2.097(4)	Ni(1)-N(6)	2.102(12)	Ni(2)-N(1)	2.122(12)
Ni(1)-N(2)	1.999(4)	Ni(1)-N(5)	1.987(12)	Ni(2)-N(2)	2.007(12)
Ni(1)-N(3)	2.080(4)	Ni(1)-N(4)	2.115(12)	Ni(2)-N(3)	2.143(13)
Ni(1)-Cl(1)	2.3444(16)	Ni(1)-Br(3)	2.458(3)	Ni(2)-Br(3)	2.471(3)
Ni(1)-Cl(2)	2.428(2)	Ni(1)-Br(1)	2.646(3)	Ni(2)-Br(2)	2.646(3)
Ni(1)-O(1)	2.117(5)	Ni(1)-O(1)	2.055(10)	Ni(2)-O(2)	2.105(10)
C(13)-N(1)	1.305(6)	C(13)-N(6)	1.256(18)	C(33)-N(1)	1.279(18)
N(3)-N(3A)	1.368(7)	N(3)-N(4)	1.347(14)		
Ni(1)···Ni(1A)	3.437	Ni(1)···Ni(2)	3.569		
Bond angles					
N(1)-Ni(1)-N(2)	79.69(18)	N(6)-Ni(1)-N(5)	77.4(5)	N(1)-Ni(2)-N(2)	79.6(5)
N(1)-Ni(1)-N(3)	154.87(17)	N(6)-Ni(1)-N(4)	153.8(5)	N(1)-Ni(2)-N(3)	154.4(5)
N(1)-Ni(1)-Cl(1)	102.08(14)	N(6)-Ni(1)-Br(3)	104.1(4)	N(1)-Ni(2)-Br(3)	103.1(4)
N(1)-Ni(1)-Cl(2)	95.97(13)	N(6)-Ni(1)-Br(1)	96.9(4)	N(1)-Ni(2)-Br(2)	97.6(3)
N(1)-Ni(1)-O(1)	93.88(17)	N(6)-Ni(1)-O(1)	90.9(4)	N(1)-Ni(2)-O(2)	91.6(4)
Cl(1)-Ni(1)-Cl(2)	92.74(5)	Br(3)-Ni(1)-Br(1)	93.16(9)	Br(3)-Ni(2)-Br(2)	91.96(9)
Cl(2)-Ni(1)-O(1)	170.11(12)	Br(1)-Ni(1)-O(1)	171.8(3)	Br(2)-Ni(2)-O(2)	170.8(3)
Ni(1)-Cl(1)-Ni(1A)	94.30(8)	Ni(1)-Br(3)-Ni(2)	92.80(8)		

[a] Atoms with suffix A are generated by symmetry (-x+1, y, -z+1/2).

Like **1** and **2**, **3a** and **3b** are paramagnetic displaying magnetic moments of *ca.* 4.2 BM (Evans Balance at ambient temperature), their values being consistent with two non-interacting high spin Ni(II) (S = 1)-Ni(II) (S = 1) metal centres (using $\mu^2 = \sum\mu_i^2$, where μ_i is the magnetic moment of the individual metal centres) [20]. The FAB mass spectra show a peak corresponding to the cationic unit minus any water molecules, [(**L**)Ni_2X_3], along with fragmentation peaks due to [(**L**)NiX_2] and [(**L**)NiX]. In the IR spectra the $\upsilon(C{=}N)_{imine}$ stretches are visible at *ca.* 1593 cm^{-1} and support metal coordination.

2.2.3. Zinc(II) chloride complexes (4)

In an attempt to make a diamagnetic analogue of chloride derivatives **1a**, **2** or **3a**, the reaction of **L** with $ZnCl_2$, under similar reaction conditions was undertaken. On work-up, [(**L**)Zn_2Cl_4] (**4b**) was isolated in reasonable yield as pale yellow crystals (Scheme 2). Complex **4b** has been characterised using FAB mass spectrometry, IR and ^{1}H NMR spectroscopy and single crystal X-ray diffraction (see experimental section).

A view of **4b** is given in Figure 6; selected bond distances and angles are compiled in Table 5. The structure comprises a neutral bimetallic complex in which one zinc centre (Zn(2)) fills a

bidentate pyridylimine binding site in **L** while the other (Zn(1)) occupies a tridentate phthalazine-pyridylimine site. The coordination sphere at each metal centre is completed by two chloride ligands to give a tetrahedral geometry at Zn(2) and a distorted square based pyramidal geometry at Zn(1) ($\tau = 0.31$) [19]. The unsymmetrical binding of zinc atoms has the result that one $N(3)_{phth}$ donor atom remains uncoordinated. Both bound pyridylimine moieties are *quasi*-planar [*tors*.: N(5)-C(15)-C(13)-N(6) 6.6°; N(1)-C(33)-C(32)-N(2) 5.9°] and are oriented essentially orthogonally to the *N*-aryl groups [*tors*.: C(33)-N(1)-C(35)-C(36) 77.6°; C(13)-N(6)-C(1)-C(2) 90.7°]. In contrast the bound phthalzine-pyridine section of the **L** shows some deviation from planarity [*tors*.: N(5)-C(19)-C(20)-N(4) 29.1°]. This deviation appears to have some significant effects on the Zn(1)-N distances with the distance to the phthalazine nitrogen being notably the longest of the exterior nitrogen donors [Zn(1)-N(4) 2.341(5) *vs.* Zn(1)-N(6) 2.216(5) Å] and moreover at the top end of the range when compared with structurally related species containing the five-coordinate (N,N_{py},N_{im})zinc dichloride motif [21]. The absence of a halide bridge, as in **1** and **2**, results in the metal centres being located far apart [Zn(1)···Zn(2) 7.123(5) Å]. There are no intermolecular contacts of note.

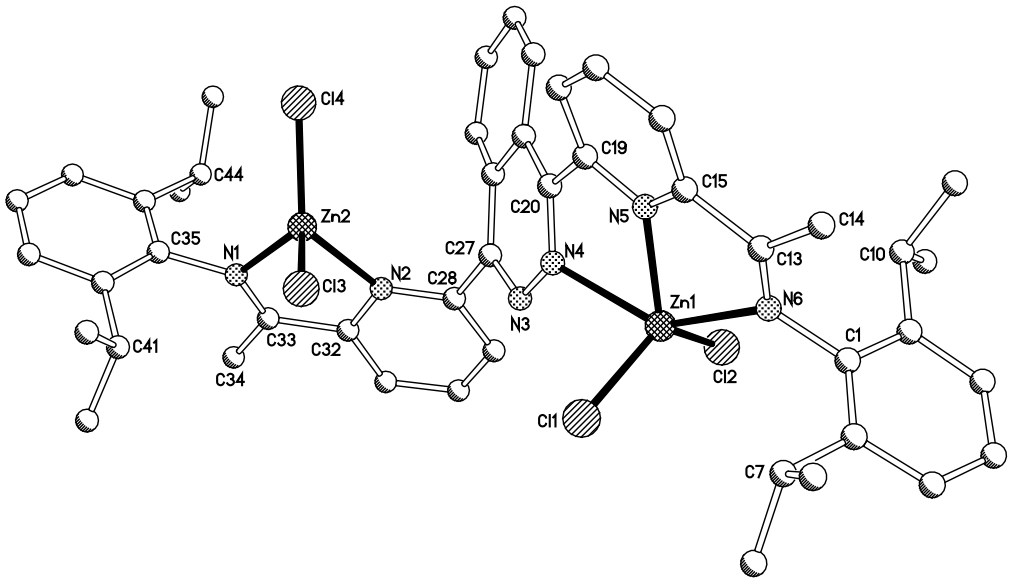

Fig. 6. Molecular structure of [(**L**)Zn_2Cl_4] (**4b**) with partial atom labeling scheme; all hydrogen atoms have been omitted for clarity

Table 5
Selected bond distances (Å) and angles (°) for **4**

Bond lengths			
Zn(1)-N(6)	2.216(5)	Zn(2)-N(1)	2.052(5)
Zn(1)-N(5)	2.094(5)	Zn(2)-N(2)	2.103(5)
Zn(1)-N(4)	2.340(5)	Zn(2)-Cl(3)	2.225(2)
Zn(1)-Cl(1)	2.2358(19)	Zn(2)-Cl(4)	2.1759(18)
Zn(1)-Cl(2)	2.2113(18)	C(33)-N(1)	1.272(7)
C(13)-N(6)	1.254(7)	Zn(1)···Zn(2)	7.123
Bond angles			
N(4)-Zn(1)-N(6)	144.96(17)	Cl(1)-Zn(1)-Cl(2)	126.02(7)
N(4)-Zn(1)-N(5)	71.22(18)	N(1)-Zn(2)-N(2)	78.9(2)
N(4)-Zn(1)-Cl(1)	95.42(14)	N(1)-Zn(2)-Cl(3)	114.26(15)
N(4)-Zn(1)-Cl(2)	92.30(14)	N(1)-Zn(2)-Cl(4)	116.92(15)
N(5)-Zn(1)-N(6)	74.17(18)	N(2)-Zn(2)-Cl(3)	102.03(14)
N(5)-Zn(1)-Cl(1)	109.88(15)	N(2)-Zn(2)-Cl(4)	125.60(14)
N(5)-Zn(1)-Cl(2)	123.10(15)	Cl(3)-Zn(2)-Cl(4)	114.24(7)

Interestingly, the room temperature ^{1}H NMR spectrum of bimetallic **4b** in CD_3CN is not supportive of the solid state structure being maintained in solution (Figure S7 in ESI). Indeed, a single type of C*Me*=N group and three types of pyridyl-H protons are evident (albeit broad), while the isopropyl CH*Me*$_2$ protons appear as just one pair of doublets (J(HH) = 6.9 Hz). Unfortunately, cooling the NMR solution to as low as -41 °C did not shed any light on the potential dynamic process occurring, instead only further broadening of the signals was observed. A possible mechanism involving flipping of the central phthalazinyl unit between coordination and non-coordination is illustrated in Scheme 3; notably the long N_{phth}-Zn distance observed in the solid state (*vide supra*) lends some support to this proposed lability. Indeed we have previously observed a related process occurring in [{bis(arylimino)terpyridine}Zn_2Cl_4].[18b]

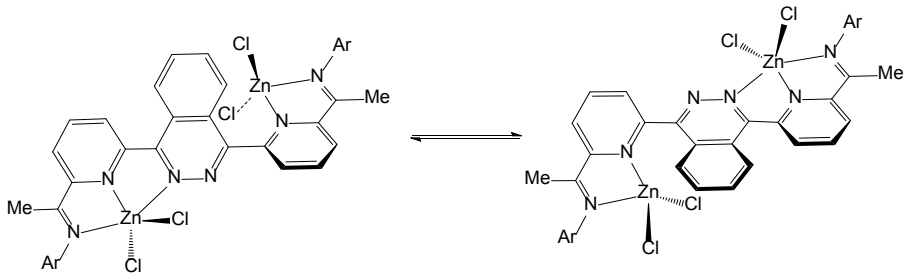

Scheme 3. Possible dynamic process occurring in solution for **4b** (Ar = 2,6-*i*-$Pr_2C_6H_3$)

The presence of inequivalent binding sites in **4b** also prompted us to explore the possibility of introducing the $ZnCl_2$ units sequentially on the ligand framework. Hence reaction of **L** with

of 1.2 equivalents of $ZnCl_2$ in *n*-BuOH at elevated temperature gave, on crystallisation from bench acetonitrile, [(**L**)$ZnCl_2$] (**4a**) as pale green crystals in moderate yield (Scheme 2). **4a** could then be readily converted to **4b** by reaction with a further equivalent of $ZnCl_2$ in acetonitrile at room temperature.

Monometallic **4a** is fluxional. At -38 °C, the ^{1}H NMR spectrum in CD_3CN shows two singlets for the inequivalent imine methyl groups and two distinct septets for the C*H*Me_2 groups; these signals coalesce at 9 °C ($\Delta G^{\ddagger}$ = 55 kJ mol^{-1} at 282 K) (Figure S8 in ESI).[22] At room temperature the ^{1}H NMR spectrum remains broad but resolves itself at 74 °C with a sharp singlet for the imine methyl group and a single well-defined septet for the C*H*Me_2 protons. Evidently there is an interchange in coordination of the pyridylimine donors within **L** (Scheme 4).

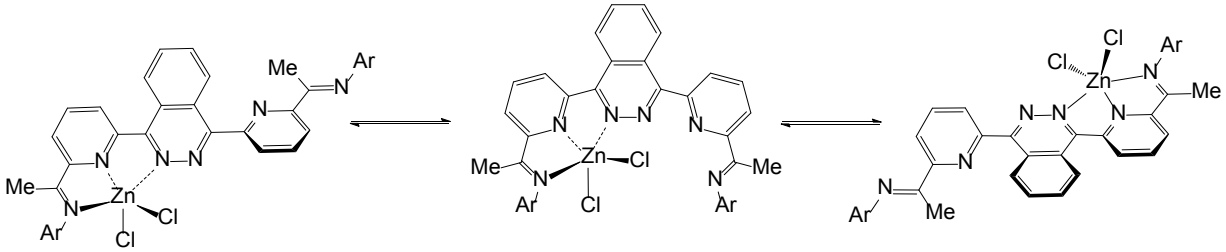

Scheme 4. Process accounting for the observed fluxionality displayed by **4a** in solution (Ar = 2,6-*i*-$Pr_2C_6H_3$)

2.3. Catalytic evaluation

Complexes **1** - **3** have all been screened as precatalysts [using methylaluminoxane (MAO) as co-catalyst] for oligomerisation of ethylene; the results are summarised in Table 6 (runs 1 - 5). All the systems showed modest activity affording hydrocarbon-based waxes that were readily soluble in toluene (and chloroform). No evidence for higher molecular weight polymeric materials could be detected under these experimental conditions.

Table 6
Catalytic evaluation of **1** – **3** for ethylene oligomerisation[a]

Run	Pre-catalyst	Mass of oligomer[b] (g)	Activity (g.mmol^{-1}.h^{-1}.bar^{-1})	Olefinic product,[c] (%)				α[d]
				α-olefin	internal	vinylidene	tri-substituted	
1	**1a** (Co)	0.051	5	39.7	36.9	4.3	19.0	-
2	**1b** (Co)	0.049	5	40.2	37.5	1.1	21.2	-
3	**2** (Fe)	0.065	7	98.5	1.5	-	-	0.66
4	**3a** (Ni)	0.142	14	25.4	74.6	-	-	-
5	**3b** (Ni)	0.134	13	26.8	73.2	-	-	-

[a] General conditions: 1 bar ethylene Schlenk test carried out in toluene (40 mL) at ambient temperature using 6.0 mmol MAO (600 eq.), 0.01 mmol pre-catalyst, over 60 min. Reactions were terminated by addition of dilute HCl.
[b] Mass of oligomer isolated.
[c] Product percentages calculated *via* integration of their ^{1}H NMR spectra.
[d] Determined from GC; α = (rate of propagation)/((rate of propagation) + (rate of chain transfer)) = (moles of C_{n+2})/(moles of C_n)

The nickel-based **3**/MAO (runs 4 and 5) proved the most active producing internal olefins as the major component of the mixture and α-olefins as the minor one. In addition, the $^{13}C\{^1H\}$ NMR spectrum of these oligomeric products indicates the presence of mainly methyl branches, along with very low levels of longer chain branches (*e.g.*, ethyl and propyl) [23]. A chain-walking mechanism has been previously used to account for the observed isomerisation/branching in related nickel-based catalysts [24]. By contrast, the cobalt systems (runs 1 and 2) were the least active resulting in extensive isomerisation to give mixtures of terminal, internal and branched products such as vinylidenes and tri-substituted materials. On the other hand, the iron system (**2**: run 3) was the most selective forming high levels of α-olefins (in the range C_4 to C_{26} from GC), a characteristic of iron oligomerisation catalysts [25].

Despite the structural similarity of the two *N,N,N*-Fe binding sites in **2** to that found in the well-documented mononuclear bis(imino)pyridine- and imino-bipyridine–iron oligomerisation catalysts [25], it is unclear as to why the performance of **2**, under comparable conditions, has proved significantly inferior. However, the observed distortions (and implications on strain) within the coordinated dinitrogen-containing heterocyclic unit in dicobalt (**1**) and dinickel species (**3**) (see Figs. 3-5), may provide some insight. It would seem plausible that a similar strain would exist in **2** giving rise to ineffective N_{phth}-Fe binding leading, under polymerisation conditions, to partial or complete dissociation in a manner similar to that seen for dizinc-

containing **4b**. It is noteworthy that the related bis(bidentate) diron system, [2,6-{(2,6-*i*-$Pr_2C_6H_3$)N=C(Me)C_5H_3N}$_2C_6H_3N$]$FeCl_2$/MAO is inactive in alkene oligomerisation [11].

3. Conclusions

The sterically bulky bis(aryliminopyridyl)phthalazine compound, **L**, has been successfully prepared and its capacity to act as a compartmental ligand demonstrated. For cobalt, nickel and iron, **L** behaves as a bis(tridentate) ligand allowing M···M separations of between 3.437 and 3.596 Å while for zinc, inequivalent bi- and tri-dentate binding domains are occupied; fluxional behaviour is a feature of the zinc complexes. Furthermore, the nature of the metal(II) centre influences the charge of the **L**-containing unit with dicationic, monocationic and neutral species all accessible. Their cobalt, iron and nickel halide complexes display only modest activities for ethylene oligomerisation on activation of **1** - **3** with MAO; the in-built strain within the ligand manifolds and implications on N_{phth} lability have been mentioned as possible contributing factors to the observed catalytic activity.

4. Experimental

4.1. General considerations

All operations, unless otherwise stated, were carried out under an inert atmosphere of dry, oxygen-free nitrogen using standard Schlenk and cannula techniques or in a nitrogen purged glove box. Solvents were distilled under nitrogen from appropriate drying agents [26] or were employed directly from a Solvent Purification System (Innovative Technology, Inc). The electrospray (ESI) mass spectra were recorded using a micromass Quattra LC mass spectrometer with dichloromethane or methanol as the matrix. FAB mass spectra (including high resolution) were recorded on Kratos Concept spectrometer with *m*-nitrobenzyl alcohol (NBA) as matrix. The infrared spectra were recorded in the solid state with Universal ATR sampling accessories on a Perkin Elmer Spectrum One FTIR instrument. NMR spectra were recorded on a Bruker DPX 300 spectrometer operating at 300.03 (^{1}H) and 75.4 MHz (^{13}C) or a Bruker DRX400

spectrometer at 400.13 (^{1}H) and 100.61 MHz (^{13}C) at ambient temperature unless otherwise stated; chemical shifts (ppm) are referred to the residual protic solvent peaks and coupling constants are expressed in hertz (Hz). Magnetic susceptibility studies were performed using an Evans Balance (Johnson Matthey) at room temperature. The magnetic moments were calculated following standard methods [27] and corrections for underlying diamagnetism were applied to the data [28]. Melting points (mp) were measured on a Gallenkamp melting point apparatus (model MFB-595) in open capillary tubes and were uncorrected. Elemental analyses were performed at the Science Technical Support Unit, London Metropolitan University.

The reagents 2,6-diisopropylaniline, phosphorus pentabromide, carbon tetrabromide, 1,4-phthalahydrazide, the metal salts [$CoCl_2$, $CoBr_2$, $FeCl_2$, $NiBr_2$(DME), $ZnCl_2$] and methylaluminoxane (MAO, 10 wt. % in toluene) were purchased from Aldrich Chemical Co. and used without further purification. The compounds tetrakis(triphenylphosphine)palladium(0) [29], 6-tributylstannyl-2-(2-methyl-1,3-dioxolan-2-yl)pyridine [18a,30] and $NiCl_2$(DME) [31] were prepared using literature procedures. All other chemicals were obtained commercially and used without further purification.

4.2. Synthesis of 1,4-dibromophthalazine

The title compound was prepared using a modification of a previously reported procedure [32]. To a round bottomed flask equipped with a stir bar and reflux condenser was added a mixture of 1,4-phthalhydrazide (1.375 g, 8.49 mmol) and carbon tetrabromide (85 g). The reaction mixture was heated to 80 °C and phosphorous pentabromide (9.135 g, 21.2 mmol, 2.5 eq.) introduced. The temperature was then raised to 130 °C and stirred at this temperature for 6 h. After cooling to room temperature, the solid mass was treated with CH_2Cl_2 (60 mL) until all lumps had been disintegrated to form a suspension. This mixture was then added to ice water (250 mL) and stirred overnight. The organic layer was extracted and dried over magnesium sulphate. Following filtration, the filtrate was concentrated until a paste was formed; the paste was filtered and washed with copious amounts of hexane. The crude product was recrystallised from hot THF and left to

stand at -30 °C overnight. The yellow needles were collected and dried; additional crops of the product were combined (71%, 1.721 g). Mp: 156-158 ºC (lit. [32]: 160 °C). ^{1}H NMR (300 MHz, $CDCl_3$, 298 K): δ 8.05 (dd, *J*(HH) 6.3, 3.0, Ar-H), 8.29 (dd, *J*(HH) 6.3, 3.0, Ar-H). IR (cm^{-1}) 2353 (br s), 1873 (br m), 1601 (w), 1558 (m), 1496 (w), 1471 (s), 1404 (s), 1344 (m), 1295 (s), 1255 (s), 1151 (w), 1139 (w), 1055 (w), 993 (s), 944 (m), 796 (s), 773 (s). FABMS: *m/z* 288 $[M]^+$. HRMS (FAB): calcd for $C_8H_5N_2{}^{79}Br_2$ $[M + H]^+$ 286.88195, found 286.88190.

4.3. Synthesis of 1,4-{(O=CMe)C_5H_3N}$_2C_8H_4N_2$

An oven-dried Schlenk flask equipped with a magnetic stir bar was evacuated and backfilled with nitrogen. The flask was charged with 1,4-dibromophthalazine (1.30 g, 4.52 mmol), 6-tributylstannyl-2-(2-methyl-1,3-dioxolan-2-yl)pyridine (4.51 g, 9.94 mmol, 2.2 equiv.), tetrakis(triphenylphosphine)palladium(0) (0.42 g, 0.36 mmol, 0.08 equiv.), cuprous bromide (0.104 g, 0.72 mmol, 0.16 equiv.) and toluene (50 mL). The reaction mixture was stirred and heated to 100 °C for 72 h. After removal of the solvent under reduced pressure, the resulting oil was stirred for 12 h in 4M HCl (50 mL). On cooling to room temperature, the reaction mixture was neutralised with sodium hydrogen carbonate and extracted with chloroform (3 x 40 mL). The combined organic extracts washed with water (3 x 40 mL), a saturated solution of the disodium salt of EDTA (2 x 30 mL) and brine (1 x 50 mL) and then dried over magnesium sulphate. Following filtration, the solvent was removed under reduced pressure and the crude product crystallised from ethanol at -30 °C to give 1,4-{(O=CMe)$_2C_5H_4N_2$}$_2C_8H_4N_2$ as a pale yellow solid (72%, 1.21 g). Mp: 167–169 ºC. ^{1}H NMR (300 MHz, $CDCl_3$, 298 K): δ 2.81 (s, 6H, C(O)CH_3), 7.99 (dd, *J*(HH) 7.2, 3.3, 2H, phth-H), 8.15 (t, *J*(HH) 7.5, 2H, Py-H), 8.25 (d, *J*(HH) 7.5, 2H, Py-H), 8.55 (d, *J*(HH) 7.5, 2H, Py-H), 8.98 (dd, *J*(HH) 7.2, 3.3, 2H, phth-H). ^{13}C{^{1}H} NMR (75 MHz, $CDCl_3$, 298 K): δ 24.9 (C(O)CH_3), 120.9 (Py-CH/phth-CH), 125.2 (phth-C), 125.9 (Py-CH/phth-CH), 128.1 (Py-CH/phth-CH), 131.4 (Py-CH/phth-CH), 137.3 (Py-CH/phth-CH), 151.5 (Py-CN/phth-CN), 154.2 (Py-CN/phth-CN), 155.2 (Py-CN/phth-CN), 198.6 (C(O)CH_3). IR (cm^{-1}) 2941 (w), 1708 (s, C=O), 1583 (s, C=N_{py}), 1451 (w), 1376 (s), 1353 (s),

1294 (m), 1239 (m), 1214 (m), 1154 (w), 1075 (s), 1025 (s), 993 (s), 818 (s), 768(m), 750 (w), 733 (s), 694 (m), 678 (m). FABMS: *m/z* 369 $[M]^+$. HRMS (FAB): calcd for $C_{22}H_{17}N_6O_2$ $[M]^+$ 369.13515, found 369.13521.

*4.4. Synthesis of 1,4-{(2,6-i-Pr$_2$C$_6$H$_3$)N=CMe)C$_5$H$_3$N}$_2$C$_8$H$_4$N$_2$ (**L**)*

1,4-{(O=CMe)C_5H_3N}$_2C_8H_4N_2$ (0.340 g, 0.92 mmol) was suspended in an excess of 2,6-diisopropylaniline (1.76 mL, 9.31 mmol, 10 eq.) and stirred for 15 min at 230 °C on a heating mantle until dissolution. A catalytic amount of formic acid was added, and the reaction mixture was stirred for an additional 20 min at 230 ºC. Following removal of the excess 2,6-diisopropylaniline under reduced pressure (130 °C, 0.5 mmHg), the resulting brown residue was stirred in ethanol at room temperature and the resultant precipitate filtered and washed with ethanol to give **L** as brown powder (83%, 0.529 g). Mp: 244-246 ºC. ^{1}H NMR (300 MHz, $CDCl_3$, 298 K): δ 1.11 (d, *J*(HH) 6.6, 12H, CH(C*H*$_3$)$_2$), 1.13 (d, *J*(HH) 6.7, 12H, CH(C*H*$_3$)$_2$), 2.21 (s, 6H, C*H*$_3$C=N), 2.71 (sept, *J*(HH) 6.6, 4H, C*H*(CH$_3$)$_2$), 7.01 – 7.19 (m, 6H, Ar-H), 7.83 (dd, *J*(HH) 7.2, 3.3, 2H, phth-H), 8.11 (t, *J*(HH) 3.9, 2H, Py-H), 8.39 (d, *J*(HH) 7.8, 2H, Py-H), 8.50 (d, *J*(HH) 8.1, Py-H), 8.95 (dd, *J*(HH) 7.2, 3.3, 2H, phth-H). ^{13}C{^{1}H} NMR (75 MHz, $CDCl_3$, 298 K): δ 17.3 ((CH$_3$)C=N), 21.8 (CH$_3$), 22.2 (CH$_3$), 27.3 (*C*H(CH$_3$)$_2$), 120.0 (CH, phth-CH/Py-CH), 122.6 (Ar-CH), 122.7 (Ar-CH), 125.3 (phth-C), 125.8 (Py-CH/phth-CH), 126.2 (Py-CH/phth-CH), 131.1 (Py-CH/phth-CH), 134.8 (Ar-CH), 136.8 (Py-CH/phth-CH), 145.3 (Ar-CN), 153.8 (phth-CN/Py-CN), 154.8 (phth-CN/Py-CN), 155.7 (Py-CN/phth-CN), 165.9 ((CH$_3$)*C*=N). IR (cm^{-1}): 2963 (m), 1645 (s, C=N$_{im}$), 1569 (s, C=N$_{py}$), 1463 (m), 1437 (s), 1383 (s), 1364 (s), 1302 (m), 1241 (m), 1192 (m), 1156 (w), 1113 (s), 1083 (m), 1044 (m), 991 (m), 936 (w), 849 (w), 825 (s), 764 (m), 748 (m), 694 (m), 668 (w). ESIMS: *m/z* 687 $[M+H]^+$. HRMS (FAB): calcd for $C_{46}H_{51}N_6$ $[M + H]^+$ 687.41752, found 687.41760.

*4.5. Synthesis of [(**L**)$Co_2X(\mu\text{-}X)(NCMe)_m(OH_2)_n$]($CoX_4$) (**1**)*

(a) X = Cl, *m* = 2, *n* = 1 (**1a**): An oven-dried Schlenk flask equipped with a magnetic stir bar was evacuated and backfilled with nitrogen. The flask was charged with $CoCl_2$ (0.056 g, 0.43 mmol) in *n*-BuOH (10 mL) and the contents stirred at 95 °C until the cobalt salt had completely dissolved. **L** (0.100 g, 0.14 mmol) was added and the reaction mixture stirred at 95 °C overnight. After cooling to room temperature, the solvent was concentrated under reduced pressure and hexane added to induce precipitation. Following filtration, washing with hexane and drying under reduced pressure, the crude product was obtained as a deep green powder (80%, 0.125 g). Recrystallisation by prolonged standing of a concentrated acetonitrile solution at room temperature gave [(**L**)$Co_2Cl(\mu\text{-}Cl)(NCMe)_2(OH_2)$]($CoCl_4$) (**1a**) as green plates. IR (cm^{-1}): 2959 (m), 2923 (s), 2851 (s), 2288 (w, $\upsilon(C{\equiv}N)_{MeCN}$), 1613 (m, $\upsilon(C{=}N)_{im}$), 1569 (w, $\upsilon(C{=}N)_{py}$), 1465 (s), 1376 (s), 1276 (m), 1200 (m), 1103 (w), 1027 (s), 941 (w), 911 (w), 850 (w), 823 (s), 799 (s), 759 (s), 747 (s), 718 (w) and 694 (s). FABMS positive: *m/z* 874 [(**L**)Co_2Cl_2], 839 [{(**L**)Co_2Cl}+H], 780 [(**L**)CoCl], 745 [(**L**)Co]. FABMS negative: *m/z* 166 [$CoCl_3$]. Anal Calc. for ($C_{46}H_{50}Cl_6Co_3N_6{\cdot}1.5H_2O$): C, 50.07; H, 4.84; N, 7.62. Found: C, 50.12; H, 5.19; N, 7.31%. μ_{eff} (Evans Balance): 5.8 BM.

(b) X = Br, *m* = 2, *n* = 0 (**1b**): Employing a similar approach to that described for **1a** using anhydrous $CoBr_2$ (0.096 g, 0.439 mmol) and **L** (0.100 g, 0.15 mmol) afforded the crude product as a brown solid (59%, 0.119 g). Recrystallisation by prolonged standing of a concentrated acetonitrile solution at room temperature gave [(**L**)$Co_2Br(\mu\text{-}Br)(NCMe)_2$]($CoBr_4$) (**1b**) as orange/brown plates. IR (cm^{-1}): 2960 (s), 2922 (s), 2853 (m), 2288 (w, $\upsilon(C{\equiv}N)_{MeCN}$), 1604 (m, $\upsilon(C{=}N)$), 1587 (w, $\upsilon(C{=}N)_{py}$), 1569 (w), 1557 (w), 1522 (w), 1464 (s), 1444 (s), 1379 (s), 1368 (s), 1311 (m), 1292 (w), 1273 (m), 1255 (w), 1198 (m), 1181 (w), 1150 (w), 1110 (w), 1055 (m), 1042 (w), 1028 (s), 937 (w), 912 (w), 884 (w), 844 (w), 828 (w), 804 (s), 783 (s), 765 (s), 750 (w), 742 (w), 731 (s), 699 (s) and 684 (s). FABMS positive: *m/z* 964 [(**L**)Co_2Br_2], 885 [(**L**)Co_2Br], 826 [(**L**)CoBr], 745 [(**L**)Co]. FABMS negative: *m/z* 298 [$CoBr_3$]. Anal Calc. for

($C_{46}H_{50}Br_6Co_3N_6 \cdot 3H_2O$): C, 39.54; H, 4.04; N, 6.01. Found: C, 39.26; H, 3.86; N, 5.85%. μ_{eff} (Evans Balance): 5.9 BM.

*4.6. Synthesis of [(**L**)$Fe_2Cl(\mu\text{-}Cl)(NCMe)_2$]($FeCl_4$) (**2**)*

An oven-dried Schlenk flask equipped with a magnetic stir bar was evacuated and backfilled with nitrogen. The flask was charged with $FeCl_2$ (0.055 g, 0.437 mmol) in *n*-BuOH (10 mL) and the contents stirred at 95 °C until the iron salt had completely dissolved. **L** (0.100 g, 0.146 mmol) was added and the reaction mixture stirred at 95 °C overnight. After cooling to room temperature, the solvent was concentrated and hexane added to precipitate the product. The suspension was filtered and dried to afford the crude product as a navy blue powder (82%, 0.127 g). The solid was dissolved in dichloromethane, filtered and layered with hexane and left to stand at room temperature to give [(**L**)$Fe_2Cl(\mu\text{-}Cl)(OH_2)_2$]($FeCl_4$) (**2**) as a blue-black microcrystalline powder. IR (cm^{-1}): 2962 (m), 1618 (m), 1585 (s, C=N_{im}), 1570 (s, C=N_{py}), 1456 (s), 1439 (s), 1376 (s), 1259 (w), 1194 (s), 1097 (m), 1057 (s), 1022(s), 865 (m), 764 (m), 741 (m), 693 (m). FABMS positive: *m/z* 905 [(**L**)Fe_2Cl_3], 869 [(**L**)Fe_2Cl_2], 777 [(**L**)FeCl]. FABMS negative: *m/z* 161 [$FeCl_3$]. Anal Calc. for ($C_{46}H_{50}Cl_6Fe_3N_6 \cdot 3OH_2 \cdot 2CH_2Cl_2 \cdot 0.5C_6H_{14}$): C, 45.91; H, 5.06; N, 6.30. Found: C, 45.90; H, 4.91; N, 5.99%.

*4.7. Synthesis of [(**L**)$Ni_2X_2(\mu\text{-}X)(OH_2)_2$](X) (**3**)*

(a) X = Cl (**3a**): An oven-dried Schlenk flask equipped with a magnetic stir bar was evacuated and backfilled with nitrogen. The flask was charged with $NiCl_2$(DME) (0.064 g, 0.292 mmol) in *n*-BuOH (10 mL) and the contents stirred at 95 °C until the nickel salt had partially dissolved. **L** (0.100 g, 0.146 mmol) was added and the reaction mixture stirred at 95 °C overnight. After cooling to room temperature, the solvent was concentrated and hexane added to precipitate the product. The suspension was filtered and dried to afford the crude product as a red-brown powder (75%, 0.111 g). Recrystallisation by prolonged standing of an acetonitrile solution at room temperature gave [(**L**)$Ni_2Cl_2(\mu\text{-}Cl)(OH_2)_2$](Cl) (**3a**) as red-brown blocks. IR (cm^{-1}): 2951

(s), 1609 (m), 1589 (s, C=N_{im}), 1565 (s, C=N_{py}), 1464 (s), 1441 (m), 1372 (s), 1307 (m), 1272 (m), 1193 (s), 1054 (w), 1032 (s), 936 (w), 817 (m), 796 (s), 760 (s). FABMS positive: *m/z* 909 [(**L**)Ni_2Cl_3], 875 [(**L**)Ni_2Cl_2], 839 [(**L**)Ni_2Cl], 781 [(**L**)NiCl], 745 [(**L**)Ni]. Anal Calc. for ($C_{46}H_{50}Cl_4N_6Ni_2 \cdot 4H_2O$): C, 54.26; H, 5.74; N, 8.25. Found: C, 54.31; H, 5.85; N, 7.99%. μ_{eff} (Evans Balance): 4.1 BM.

(b) X = Br (**3b**): Employing a similar procedure to that described for **3a** using $NiBr_2$(DME) (0.090 g, 0.292 mmol), **L** (0.100 g, 0.146 mmol) and *n*-BuOH (10 mL) gave the crude product as a pale brown powder (57%, 0.111 g). Recrystallisation by prolonged standing of an acetonitrile solution at room temperature gave [(**L**)Ni_2Br_2(μ-Br)$(OH_2)_2$](Br) (**3b**) as red-brown needles. IR (cm^{-1}): 2952 (s), 1611 (m), 1588 (s, C=N_{im}), 1569 (s, C=N_{py}), 1465 (s), 1441 (m), 1371 (s), 1309 (m), 1273 (m), 1194 (s), 1101 (w), 1055 (w), 1034 (s), 937 (w), 818 (m), 795 (s), 759 (s). FABMS positive: *m/z* 1043 [(**L**)Ni_2Br_3], 964 [(**L**)Ni_2Br_2], 883 [(**L**)Ni_2Br], 825 [(**L**)NiBr], 825 [(**L**)Ni]. Anal Calc. for ($C_{46}H_{50}Br_4N_6Ni_2 \cdot 6H_2O$): C, 44.84; H, 5.07; N, 6.82. Found: C, 45.00; H, 4.71; N, 6.51%. μ_{eff} (Evans Balance): 4.3 BM.

*4.8. Synthesis of [(**L**)$ZnCl_2$] (**4a**)*

An oven-dried Schlenk flask equipped with a magnetic stir bar was evacuated and backfilled with nitrogen. The flask was charged with $ZnCl_2$ (0.024 g, 0.175 mmol) in *n*-BuOH (10 mL) and the contents stirred at 95 °C until the zinc salt had completely dissolved. **L** (0.100 g, 0.14 mmol) was added and the reaction mixture stirred at 95 °C for 4 h. After cooling to room temperature, the solvent was concentrated and hexane added to precipitate the product. The suspension was filtered and dried to afford the crude product as pale green microcrystalline solid (52%, 0.062 g). Recrystallisation from warm acetonitrile gave [(**L**)$ZnCl_2$] (**4a**) as pale green crystals. ^{1}H NMR (400 MHz, CD_3CN, 235 K): δ 1.06 (d, *J*(HH) 6.8, 6H, CH(CH_3)$_2$), 1.11 (d, *J*(HH) 7.2, 6H, CH(CH_3)$_2$), 1.13 (d, *J*(HH) 7.2, 6H, CH(CH_3)$_2$), 1.25 (d, *J*(HH) 6.8, 6H, CH(CH_3)$_2$), 2.22 (s, 3H, CH_3C=N), 2.49 (s, 3H, CH_3C=N), 2.80 (sept, *J*(HH) 6.8, 2H, C*H*(CH_3)$_2$), 3.06 (sept, *J*(HH) 6.8,

2H, C*H*(CH_3)$_2$), 7.13 (t, *J*(HH) 7.2, 1H, Ar-H), 7.23 (d, *J*(HH) 7.6, 2H, Ar-H), 7.33 (m, 3H, Ar-H), 8.19-8.33 (m, 4H, phth-H/Py-H), 8.53 (d, *J*(HH) 7.6, 1H, phth-H or Py-H), 8.60 (d, *J*(HH) 7.7, 1H, phth-H or Py-H), 8.65 (t, *J*(HH) 8.0, 1H, Py-H), 8.80 (m, 2H, phth-H/Py-H), 9.05 (dd, *J*(HH) 7.6, 1.6, 1H, phth-H). ^{1}H NMR (400 MHz, CD_3CN, 298 K): δ 1.11 (d, *J*(HH) 6.8, 12H, CH(C*H*$_3$)$_2$), 1.21 (d, *J*(HH) 7.2, 12H, CH(C*H*$_3$)$_2$), 2.35 (s, 6H, C*H*$_3$C=N), 2.95 (br m, 4H, C*H*(CH_3)$_2$), 7.15-7.31 (m, 6H, Ar-H), 8.12-8.22 (m, 2H, phth-H), 8.31-8.57 (m, 4H, Py-H), 8.88-8.92 (m, 2H, phth-H). IR (cm^{-1}) 1645 (m, C=N_{im}), 1620 (m, C=N_{im}), 1590 (s, C=N_{py}), 1466 (s), 1369 (s), 1381 (s), 1195 (s), 1110 (s), 802 (s), 765 (s), 750 (s), 700 (s). FABMS: *m/z* 787 [(**L**)ZnCl]. Anal Calc. for ($C_{46}H_{50}N_6Cl_2Zn$): C, 67.12; H, 6.08; N, 10.21. Found: C, 67.03; H, 5.97; N, 10.02%.

*4.9. Synthesis of [(**L**)Zn_2Cl_4] (**4b**)*

An oven-dried Schlenk flask equipped with a magnetic stir bar was evacuated and backfilled with nitrogen. The flask was charged with $ZnCl_2$ (0.059 g, 0.437 mmol) in *n*-BuOH (10 mL) and the contents stirred at 95 °C until the zinc salt had completely dissolved. **L** (0.100 g, 0.146 mmol) was added and the reaction mixture stirred at 95 °C overnight. After cooling to room temperature, the solvent was concentrated and hexane added to precipitate the product. The suspension was filtered and dried to afford the crude product as pale yellow microcrystalline solid (47%, 0.066 g). Recrystallisation from warm acetonitrile gave [(**L**)Zn_2Cl_4] (**4b**) as yellow blocks. ^{1}H NMR (400 MHz, CD_3CN, 298 K): δ 1.09 (d, *J*(HH) 6.9, 12H, CH(C*H*$_3$)$_2$), 1.20 (t, *J*(HH) 6.6, 12H, CH(C*H*$_3$)$_2$), 2.50 (s, 6H, C*H*$_3$C=N), 2.91 (sept, *J*(HH) 6.6, 4H, C*H*(CH_3)$_2$), 7.17 (m, 6H, Ar-H), 8.38 (br m, 2H, phth-H), 8.48 (d, *J*(HH) 7.8, 2H, Py-H), 8.60 (br m, 2H, Py-H), 8.75 (br m, 2H, Py-H), 8.81 (m, 2H, phth-H). IR (cm^{-1}) 1628 (m, C=N_{im}), 1611 (w), 1590 (s, C=N_{py}), 1572 (w), 1466 (s), 1441 (m), 1369 (s), 1308 (m), 1257 (m), 1198 (m), 1103 (w), 1057 (w), 1015 (m), 937 (w), 828 (s), 794 (s), 685 (s). FABMS: *m/z* 922 [(**L**)Zn_2Cl_3], 888 [(**L**)Zn_2Cl_2], 787 [(**L**)ZnCl]. Anal Calc. for ($C_{46}H_{50}N_6Cl_4Zn_2$): C, 57.58; H, 5.25; N, 8.76. Found: C, 57.67; H, 5.13; N, 8.60%.

4.10. General screening for ethylene oligomerisation

An oven dried 200 mL Schlenk vessel equipped with magnetic stir bar was evacuated and backfilled with nitrogen. The vessel was charged with the precatalyst (0.01 mmol) and dissolved or suspended in toluene (40 mL). MAO (6.0 mmol, 600 eq.) was introduced and the reaction mixture left to stir for 5 min. resulting in a colour change of the solution. The vessel was purged with ethylene and the contents magnetically stirred under 1 bar ethylene pressure at room temperature for the duration of the test. After one hour, the test was terminated by the addition of dilute aqueous hydrogen chloride (5 mL). The organic phase was separated, dried over magnesium sulfate and the solvent removed under reduced pressure. The ^{1}H NMR spectra of the residues were recorded in $CDCl_3$ while GC was performed directly on the extracted organic phase.

4.11. Crystallographic Studies

Data for **L**, **1a**, **1b**, **3a**, **3b** and **4b** were collected on a Bruker APEX 2000 CCD diffractometer. Details of data collection, refinement and crystal data are listed in Table 7. The data were corrected for Lorentz and polarisation effects and empirical absorption corrections applied. Structure solution by direct methods and structure refinement based on full-matrix least-squares on F^2 employed SHELXTL version 6.10 [33]. Hydrogen atoms were included in calculated positions (C-H = 0.93 – 1.00 Å) riding on the bonded atom with isotropic displacement parameters set to 1.5 U_{eq}(C) for methyl H atoms and 1.2 U_{eq}(C) for all other H atoms. All non-H atoms, were refined with anisotropic displacement parameters. Disordered solvent was omitted using the SQUEEZE option in PLATON for **1a**, **3a**, **3b** and **4b** [34].

Table 7
Crystallographic and data processing parameters for **L**, **1a**, **1b**, **3a**, **3b** and **4b**

Complex	**L**	**1a**	**1b**	**3a**	**3b**	**4b**
Formula	$C_{138}H_{150}N_{18}$·MeCN	$C_{50}H_{58}Cl_6Co_3N_8O_2$· 4MeCN	$C_{50}H_{56}Br_6Co_3N_9$· MeCN	$C_{46}H_{54}Cl_4N_6Ni_2O_2$· 6MeCN·24$H_2O$	$C_{46}H_{54}Br_4N_6Ni_2O_2$· MeCN·0.5$H_2O$	$C_{46}H_{50}Cl_4N_6Zn_2$· 2MeCN·2H_2O
M	2101.81	1340.75	1466.33	1660.88	1210.07	1077.60
Crystal size (mm^3)	0.27 x 0.18 x 0.11	0.22 x 0.14 x 0.06	0.18 x 0.13 x 0.02	0.42 x 0.37 x 0.31	0.08 x 0.06 x 0.03	0.20 x 0.11 x 0.09
Temperature (K)	293(K)	150(2)	150(2)	150(2)	150(2)	150(2)
Crystal system	triclinic	triclinic	triclinic	monoclinic	monoclinic	triclinic
Space group	P1	P-1	P-1	C2/c	P2(1)/c	P-1
a (Å)	8.4262(11)	10.348(7)	10.1377(12)	17.741(13)	10.128(2)	10.836(2)
b (Å)	17.168(2)	15.198(10)	15.0119(18)	29.383(13)	35.600(7)	15.500(3)
c (Å)	22.654(3)	20.775(13)	20.386(3)	14.432(8)	14.155(3)	16.158(3)

α (°)	111.459(3)	78.331(11)	94.258(2)	90	90	78.372(4)
β (°)	90.996(3)	85.330(11)	96.404(2)	102.206(14)	101.16(3)	89.035(4)
γ (°)	103.005(3)	72.248(10)	109.625(3)	90	90	74.331(5)
U (Å^3)	2953.7(7)	3047(3)	2883.3(6)	7353(7)	4989.2(17)	2557.4(9)
Z	1	2	2	4	4	2
D_c (Mg m^{-3})	1.182	1.461	1.689	1.500	1.611	1.399
F(000)	1126	1386	1450	3536	2444	1120
μ(Mo-K$_\alpha$)(mm^{-1})	0.070	1.121	5.053	0.744	4.004	1.194
Reflections collected	21607	23633	22850	28182	13672	20124
Independent reflections	10317	11805	11216	7221	9221	9917
R_{int}	0.0830	0.1154	0.0785	0.1623	0.0965	0.0886
Restraints /parameters	2415/1461	578/627	0/644	3/287	0/531	0/533
Final R indices (I>2σ(I))	R1 = 0.0654 wR2 = 0.0979	R1 = 0.0902 wR2 = 0.1974	R1 = 0.0582 wR2 = 0.0895	R1 = 0.0771 wR2 = 0.1785	R1 = 0.0915 wR2 = 0.1987	R1 = 0.0662 wR2 = 0.1289
All data	R1 = 0.1732 wR2 = 0.1306	R1 = 0.1777 wR2 = 0.2264	R1 = 0.1242 wR2 = 0.1055	R1 = 0.1523 wR2 = 0.1989	R1 = 0.2381 wR2 = 0.2348	R1 = 0.1384 wR2 = 0.1460
Goodness of fit on F^2 (all data)	0.811	0.861	0.773	0.853	0.774	0.781

Data in common: graphite-monochromated Mo-K$_\alpha$ radiation, λ = 0.71073 Å; $R_1 = \Sigma||F_o| - |F_c||/\Sigma|F_o|$, $wR_2 = [\Sigma w(F_o^2 - F_c^2)^2/\Sigma w(F_o^2)^2]^{½}$, $w^{-1} = [\sigma^2(F_o)^2 + (aP)^2]$, $P = [\max(F_o^2,0) + 2(F_c^2)]/3$, where a is a constant adjusted by the program; goodness of fit = $[\Sigma(F_o^2 - F_c^2)2/(n - p)]^{1/2}$ where n is the number of reflections and p the number of parameters.

Acknowledgements

We thank the University of Leicester for financial assistance. Johnson Matthey PLC are thanked for their generous loan of palladium chloride.

Appendix A: Supplementary material

Electronic supplementary information (ESI) available: ORTEP representations of crystal structures and selected NMR spectra including variable temperature studies of **4a**. CCDC reference numbers 1401482-1401487 contain the supplementary crystallographic data for compounds **L**, **1a**, **1b**, **3a**, **3b** and **4b**, respectively. These data can be obtained free of charge from the Cambridge Crystallographic Data Centre via www.ccdc.cam.ac.uk/data-request/cif. Supplementary data associated with this article can be found, in the online version, at http://.....

References

[1] For reviews see: (a) M. Delfero, T. J. Marks, Chem. Rev. 111 (2011) 2450;
(b) H. Makio, H. Terao, A. Iwashita, T. Fujita, Chem. Rev. 111 (2011) 2363;
(c) D. Takeuchi, Dalton Trans. 39 (2010) 311;
(d) J. P. McInnis, M. Delferro, T. J. Marks, Acc. Chem. Res. 47 (2014) 2545.

[2] A. L. Gavrilova, B. Bosnich, Chem. Rev. 104 (2004) 349.

[3] (a) M. R. Radler, T. Agapie, Organometallics 33 (2014) 3247;
(b) S. Liu, A. Motta, A. R. Mouat, M. Delferro, T. J. Marks, J. Am. Chem. Soc. 136 (2014) 10460.

[4] (a) J. D. A. Pelletier, J. Fawcett, K. Singh, G. A. Solan, J. Organomet. Chem. 693 (2008) 2723;
(b) Y. Cui, S. Zhang, W.-H. Sun, Chin. J. Polym. Sci. 26 (2008) 539;
(c) S. Jie, D. Zhang, T. Zhang, W.-H. Sun, J. Chen, Q. Ren, D. Liu, G. Zheng, W. Chen, J. Organomet. Chem. 690 (2005) 1739;
(d) Q. Xing, T. Zhao, S. Du, W. Yang, T. Liang, C. Redshaw, W.-H. Sun, Organometallics 33 (2014) 1382;
(e) L. Wang, J. Sun, Inorg. Chim. Acta 361 (2008) 1843;

(f) H.-K. Luo, H. Schumann, J. Mol. Catal. A: Chem. 227 (2005) 153;
(g) M. Tababiki, K. Tsuchiya, Y. Motoyama, H. Nagashima, Chem. Commun. (2005)3409;
(h) D. Noda, M. Tananiki, K. Tsuchiya, Y. Sunada, H. Nagashima, *Polyhedron* 28 (2009) 3935.

[5] (a) W.-H. Wang, G.-X. Jin, Inorg. Chem. Commun. 9 (2006) 548;
(b) T. Hu, Y.-G. Li, Y.-S. Li, N.-H. Lu, J. Mol. Catal. A: Chem. 253 (2006) 155;
(c) S. J. Na, D. J. Joe, S. Sujith, W.S. Han, S. O. Kang, B. Y. Lee, J. Organomet. Chem. 691 (2006) 611;
(d) S. Sujith, D. J. Joe, S. J. Na, Y.-W. Park, C. H. Choi, B. Y. Lee, Macromecules 38 (2005) 10027;
(e) D. Zhang, G.-X. Jin, Inorg. Chem. Commun. 9 (2006) 1322;
(f) P. Wehrmann, S. Mecking, Organometallics 27 (2008) 1399.

[6] X. Li, Y. Li, Y. Li, Y. Chen, N Hu, Organometallics 24 (2005) 2502.

[7] (a) G. A. Solan, J. D. A. Pelletier, PCT Int. Appl. (2005), WO 2005118605 A1 20051215. (ExxonMobil Chemical);
(b) A. P. Armitage, Y. D. M. Champouret, H. Grigoli, J. D. A. Pelletier, K. Singh, G. A. Solan, Eur. J. Inorg. Chem. (2008) 4597;
(c) Q. Khamker, Y. D. M. Champouret, K. Singh, G. A. Solan, Dalton Trans. (2009) 8935.

[8] (a) Q. Chen, J. Yu, J. Huang, Organometallics 26 (2007) 617;
(b) B. A. Rodriguez, M. Delferro, T. J. Marks, Organometallics 27 (2008) 2166.

[9] (a) R. Radlauer, M. W. Day, T. Agapie, J. Am. Chem. Soc. 134 (2012) 1478;
(b) M. R. Radlauer, A. K. Buckley, L. M. Henling, T. Agapie, J. Am. Chem. Soc. 135 (2013) 3784.

[10] (a) B. A. Rodriguez, M. Delferro, T. J. Marks, J. Am. Chem. Soc. 131 (2009) 5902;
(b) D. Takeuchi, Y. Chiba, S. Takano, K. Osakada, Angew. Chem. Int. Ed. 52 (2013) 12536;
(c) M. P. Weberski, Jr., C. Chen, M. Delferro, T. J. Marks, Chem. Eur. J. 18 (2012) 10715.

[11] Y. D. M. Champouret, J. Fawcett, W. J. Nodes, K. Singh, G. A. Solan, Inorg. Chem. 45 (2006) 9890.

[12] J. Aguilo, A. Naeimi, R. Bofill, H. Mueller-Bunz, A. Llobet, L. Escriche, X. Sala, M. Albrecht, New J. Chem. 38 (2014) 1980.

[13] T. Yamaguchi, T. Koike, M. Akita, Organometallics 29 (2010) 6493.

[14] T. J. Hebden, W. W. Brennessel, C. J. Flaschenreim, P. L. Holland, Dalton Trans. (2006) 3855.

[15] (a) A. M. Barrios, S. J. Lippard, Inorg. Chem. 40 (2001) 1060;
(b) J. Kuzelka, S. Mukhopadhyway, B. Spingler, S. J. Lippard, Inorg. Chem. 43 (2004) 1751;
(c) A. M. Barrios, S. J. Lippard, J. Am. Chem. Soc. 121 (1999) 11571;
(d) J. Kuzelka, B. Spingler, S. J. Lippard, Inorg. Chim. Acta 337 (2002) 212;
(e) C. J. Sumby, P. J. Steel, J. Coord. Chem. 61 (2008) 2179;
(f) A. M. Barrios, S. J. Lippard, J. Am. Chem. Soc. 122 (2000) 9172.

[16] S. Roggan, C. Limberg, C. Knispel, T. D. Tilley, Dalton Trans. 40 (2011) 4315.

[17] (a) H. Kon, T. Nagata, Dalton Trans. 42 (2013) 5697;
(b) Z. Deng, H.-W. Tseng, R. Zong, D. Wang, R. Thummel, Inorg. Chem. 47 (2008) 1835;
(c) Y. Xu, A. Fischer, L. Duan, L. Tong, E. Gabrielsson, B. Akermark, L. Sun, Angew. Chem., Int. Ed. 49 (2010) 8934.

[18] (a) Y. D. M. Champouret, R. K. Chaggar, I. Dadhiwala, J. Fawcett, G. A. Solan, Tetrahedron 62 (2006) 79;
(b) Y. D. M. Champouret, J.-D. Maréchal, I. Dadhiwala, J. Fawcett, D. Palmer, G. A. Solan, Dalton Trans. (2006) 2350;
(c) Y. D. M. Champouret, J.-D. Marechal, R. K. Chaggar, J. Fawcett, K. Singh, F. Maseras, G. A. Solan, New J. Chem. (2007) 75.

[19] $\tau = (\beta - \alpha)/60$ where β = the largest L-M-L angle and α = the second largest: A. W Addison, T. N. Rao, J. Reedijk, J. von Rijn, G. C. Verschoor, J. Chem. Soc., Dalton Trans. (1984)1349.

[20] A. Gerli, K. S. Hagen, L. G. Marzilli, Inorg. Chem. 30 (1991) 4673.

[21] CSD search 2015 (June): Exterior *N,N,N*-bound zinc halide complexes: range: 2.352 – 2.217 Å.

[22] Rate constants obtained from line shape analysis of the C*Me*=N ^{1}H NMR signals of **4a** were used to produce an Eyring plot, which yielded values of $\Delta G^{\ddagger}$.
[23] (a) T. Usami, S. Takayama, Macromolecules 17 (1984) 1756;
(b) G. B. Galland, R. F.de Souza, R. S. Mauler, F. F. Nunes, Macromolecules 32 (1999) 1620; (c) L. P. Linderman, N. O. Adams, Anal. Chem. 43 (1971) 1245;
(d) M. De Pooter, P. B. Smith, K. K. Dohrer, K. F. Bennett, M. D. Meadows, C. G. Smith, H. P. Schouwenaars, R. A. Geerards, J. Appl. Polym. Sci. 42 (1991) 399.
[24] (a) S. Mecking, Angew. Chem., Int. Ed. 40 (2001) 534;
(b) S. D. Ittel, L.K. Johnson, M. Brookhart, Chem. Rev. 100 (2000) 1169.
[25] (a) V. C. Gibson, C. Redshaw, G. A. Solan, Chem. Rev. 107 (2007) 1745;
(b) C. Bianchini, G. Giambastiani, G. I. Rios, G. Mantovani, A. Meli, A. M. Segarra, Coord. Chem. Rev. 250 (2006) 1391;
(c) V. C. Gibson, G. A. Solan, from Catalysis without Precious Metals (Ed. R.M. Bullock), Wiley-VCH, Weinheim, 111 (2010);
(d) V. C. Gibson, G. A. Solan, Top. Organomet. Chem. 26 (2009) 107.
[26] W. L. F. Armarego, D. D. Perrin, in 'Purification of Laboratory Chemicals', Butterworth Heinemann, 4th edn., 1996.
[27] F. E. Mabbs, D. J. Machin, 'Magnetism and Transition Metal Complexes', Chapman and Hall, London, 1973.
[28] (a) C. J. O'Connor, Prog. Inorg. Chem. 29 (1982) 203;
(b) 'Handbook of Chemistry and Physics', ed. R.C. Weast, CRC Press, Boca Raton, FL, 70th edn., 1990, p. E134.
[29] F. Tellier, R. Sauvêtre, J.-F. Normant, J. Organomet. Chem. 292 (1985) 19.
[30] R. Zong, D. Wang, R. Hammitt, R. P. Thummel, J. Org. Chem. 71 (2006) 167.
[31] A. Kermagoret, P. Braunstein, Organometallics 27 (2008) 88.
[32] A. Hirsch, D. Orphanos, Can. J. Chem. 43 (1965) 2708.
[33] G. M. Sheldrick, SHELXTL Version 6.10. Bruker AXS, Inc. Madison, Wisconsin, USA, 2000.
[34] A. L. Spek, Acta Cryst. A46 (1990) C-34.

Legends for Figures, Schemes and Tables

Fig. 1 Compartmental ligands based on 1,4-dipyridinyl-substituted phthalazines (**A**) and **L.**

Fig. 2 Molecular structure of **L** including a partial atom numbering scheme. All hydrogen atoms have been omitted for clarity.

Fig. 3 Molecular structure of the dicationic unit in **1a** including a partial atom numbering scheme. All hydrogen atoms have been omitted for clarity.

Fig. 4 Molecular structure of the dicationic unit in **1b** including a partial atom numbering scheme. All hydrogen atoms have been omitted for clarity.

Fig. 5 Molecular structures of (a) **3a** and (b) **3b**, including a partial atom numbering scheme. All hydrogen atoms, apart from those belonging to the waters, have been omitted for clarity.

Fig. 6 Molecular structure of **4b** including a partial atom numbering scheme. All hydrogen atoms have been omitted for clarity.

Scheme 1. *Reagents and conditions*: (i) $C_8H_4N_2Br_2$, $Pd(PPh_3)_4$ (8 mol%), CuBr (16 mol%), toluene, 100 °C, 72 h; (ii) HCl (4 M), 60 °C, 12 h; (iii) 2,6-*i*-$Pr_2C_6H_3NH_2$, 230 °C, cat. H^+.

Scheme 2. *Reagents and conditions*: (i) 3 CoX_2 (X = Cl, Br), *n*-BuOH, 95 °C, 12 h; (ii) MeCN-H_2O, heat; (iii) 2 NiX_2(DME) (X = Cl, Br), *n*-BuOH, 95 °C, 12 h; (iv) 2 $ZnCl_2$, *n*-BuOH, 95 °C, 12 h; (v) $ZnCl_2$, *n*-BuOH, 95 °C, 4 h; (vi) $ZnCl_2$, MeCN, RT, 12 h (Ar = 2,6-*i*-$Pr_2C_6H_3$).

Scheme 3. Possible dynamic process occurring in solution for **4b** (Ar = 2,6-*i*-$Pr_2C_6H_3$).

Scheme 4. Process accounting for the observed fluxionality displayed by **4a** in solution (Ar = 2,6-*i*-$Pr_2C_6H_3$).

Table 1 Selected bond lengths (Å) and angles (°) for **L**.

Table 2 Selected bond lengths (Å) and angles (°) for **1a**.

Table 3 Selected bond lengths (Å) and angles (°) for **1b**.

Table 4 Selected bond lengths (Å) and angles (°) for **3a** and **3b**.

Table 5 Selected bond lengths (Å) and angles (°) for **4b**.

Table 6 Catalytic evaluation of **1** – **3** for ethylene oligomerisation.[a]

Table 7 Crystallographic and data processing parameters for **L**, **1a**, **1b**, **3a**, **3b** and **4b**.